Chemistry–A European Journal
Research Article
doi.org/10.1002/chem.202300477
Chemistry Europe
European Chemical Societies Publishing
www.chemeurj.org

Design, Synthesis and Aromaticity of an Alternating Cyclo[4]Thiophene[4]Furan

Manami Kawakami+,[a] Dhruv Sharma+,[a] Anthony J. Varni,[a] Stephanie Tristram-Nagle,[b] David Yaron,[a] Tomasz Kowalewski,*[a] and Kevin J. T. Noonan*[a]

Abstract: A new class of conjugated macrocycle, the cyclo[4]thiophene[4]furan hexyl ester (C4TE4FE), is reported. This cycle consists of alternating α-linked thiophene-3-ester and furan-3-ester repeat units, and was prepared in a single step using Suzuki–Miyaura cross-coupling of a 2-(thiophen-2-yl)furan monomer. The ester side groups help promote a *syn* conformation of the heterocycles, which enables formation of the macrocycle. Cyclic voltammetry studies revealed that C4TE4FE could undergo multiple oxidations, so treatment with $SbCl_5$ resulted in formation of the $[C4TE4FE]^{2+}$ dication. Computational work, paired with ^1H NMR spectroscopy of the dication, revealed that the cycle becomes globally aromatic upon $2e^-$ oxidation, as the annulene pathway along the outer ring becomes Hückel aromatic. The change in ring current for the cycle upon oxidation was clear from ^1H NMR spectroscopy, as the protons of the thiophene and furan rings shifted downfield by nearly 6 ppm. This work highlights the potential of sequence control in furan-based macrocycles to tune electronic properties.

Introduction

Synthetic conjugated macrocycles have attracted attention for host–guest chemistry, supramolecular assemblies and as electronic materials.[1] Synthesizing these cycles purely from aromatic building blocks imparts structural rigidity, while also opening the way to redox switching between locally and globally aromatic states upon $2e^-$ oxidation or reduction.[2] The [*n*]cycloparaphenylenes (CPPs),[3] cyclo[*n*]pyrroles (CPs),[4] and cyclo[*n*]thiophenes (CTs)[5] are all well-known classes of macrocycles which were first synthesized between 15 and 25 years ago. The cyclo[*n*]furans (CFs) are a recent addition to the family (Figure 1),[6] where the small size of furan enables formation of small macrocycles (5–8 repeat units),[6] and the large rotational barriers for oligofurans[7] imparts rigidity to these π-conjugated structures.

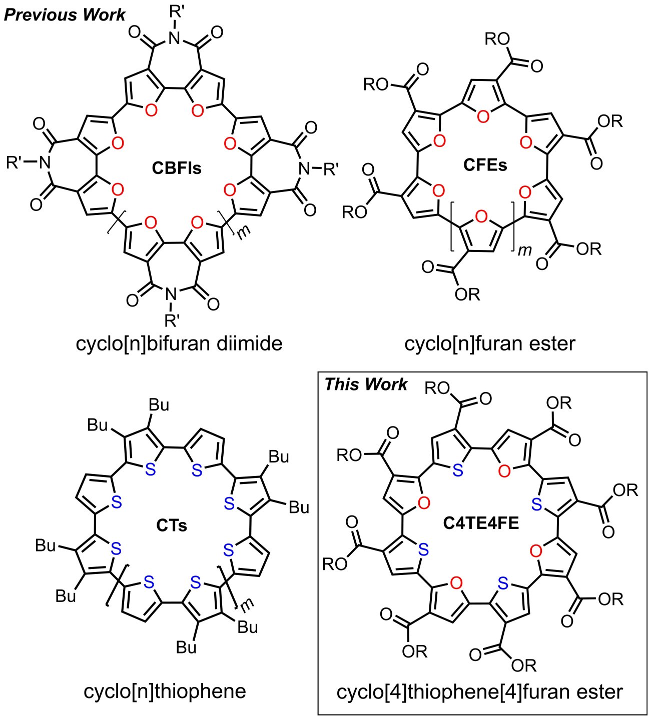

Figure 1. Previously reported furan- and thiophene-based macrocycles[5–6] and the newly synthesized alternating thiophene-furan macrocycle.

We recently discovered that ester side groups can template formation of macrocyclic[6d] and helical oligo and polyfurans[8] in a single synthetic step via cross-coupling of an appropriately functionalized monomer or dimer. Computational studies revealed that the regioregular, head-to-tail ester side groups force adjacent furan rings to adopt a *syn* configuration, driven

---

[a] M. Kawakami,+ D. Sharma,+ Dr. A. J. Varni, Prof. D. Yaron,
Prof. T. Kowalewski, Prof. K. J. T. Noonan
Department of Chemistry
Carnegie Mellon University
4400 Fifth Avenue, Pittsburgh, Pennsylvania 15213-2617 (USA)
E-mail: tomek@andrew.cmu.edu
noonan@andrew.cmu.edu

[b] Prof. S. Tristram-Nagle
Department of Physics
Carnegie Mellon University
5000 Forbes Ave, Pittsburgh, Pennsylvania 15213-2617 (USA)

[+] These authors contributed equally to this work.

Supporting information for this article is available on the WWW under https://doi.org/10.1002/chem.202300477

by intramolecular non-covalent interactions. Herein, we demonstrate that this templating effect of ester side groups is applicable to mixed thiophene-furan dimers, as we synthesized an alternating cyclo[4]thiophene[4]furan hexyl ester macrocycle in a single step (C4TE4FE, shown in Figure 1). Tuning the properties of conjugated macrocycles via sequence control has been an active area of research for several decades,[9] and this alternating cycle has unique electronic properties compared to previously synthesized CFs and CTs.

These unique electronic properties can be partially attributed to the relief of ring strain and planarization of the macrocycle. According to Gidron and coworkers, computational analysis shows that CFs with 5–7 repeat units are planar or near planar, while CTs of the same size are cone or bowl-shaped.[6a] In comparison to the strained cyclo[8]thiophene (C8T),[5b] computations predict the C4TE4FE molecule studied here to be planar, which enhances conjugation and opens the possibility of aromaticity.[10] Below, we present computational results that suggest C4TE4FE is weakly antiaromatic in its neutral state, which is as expected given that the outer pathway of carbon atoms is comprised of 16π bonds and 32π electrons (Hückel 4n system). Similarly, $2e^-$ oxidation makes C4TE4FE globally aromatic, and this is supported by both the ^{1}H NMR and absorbance spectra reported below. This is noteworthy compared to cyclo[10]thiophene (C10T), where Nucleus Independent Chemical Shift (NICS) calculations have suggested that C10T is non-aromatic.[11] Moreover, the [C10T]$^{2+}$ dication was reported to be a diradical species, with no evidence for global aromaticity despite having 38π electrons and a [40]annulene pathway of carbon atoms.[12]

Results and Discussion

In previous work we discovered that a *syn* conformation is favoured for α-linked oligofurans when decorated with head-to-tail ester side groups.[8] Here, we used torsional scans to understand how inclusion of a thiophene would impact the conformational directing effect of the ester side group. Two head-to-tail regioisomers of α-linked thiophene-3-carboxylate (TE) and furan-3-carboxylate (FE) were considered (TEFE and FETE), and these were compared to the relevant homodimers (FEFE and TETE) as shown in Figure 2. For all computed dimers, the XCCX dihedral was constrained from 0° (*syn*) to 180° (*anti*) at 15° intervals,[7f,13] with optimization of each conformer at the B3LYP-D3(BJ)/6-31G(d,p) level (Figure 2).[14] For all quantum chemical calculations, methyl ester groups were used to minimize computational cost and the *me* prefix is used to denote computed structures.

As expected from prior work, the *syn* conformation emerged as the global energy minimum for the *me*-FEFE dimer, 3.5 kcal/mol lower than the *anti* conformer (red trace, Figure 2B).[6d,8] Twisted non-planar minima were noted for the *me*-TETE derivative (blue trace, Figure 2B), where steric interactions between heteroatom lone pairs likely make the *syn* and *anti* coplanar conformations less favorable. Strikingly, the rotational barrier for the *me*-TETE derivative was ~4.5 kcal/mol lower than that of the *me*-FEFE derivative. Generally, α-linked conjugated oligothiophenes are known to twist easily from coplanarity[15] whereas the analogous oligofurans favour coplanar geometries with higher rotational barriers,[7] so the results are in line with expectation.

For the two mixed dimers, the *syn* coplanar conformation was the lowest energy conformer in both instances (purple and orange traces, Figure 2A), similar to the observation with the ester-functionalized bifuran. The rotational barriers for *me*-TEFE (5.8 kcal/mol) and *me*-FETE (6.5 kcal/mol) from the *syn* coplanar conformation are close to the values noted for the *me*-FEFE dimer (6.8 kcal/mol). Notably, the energy difference between the *syn* and *anti* coplanar forms is markedly different for *me*-TEFE and *me*-FETE. A ~6.1 kcal/mol difference in energy was noted for the *syn* and *anti* forms of *me*-TEFE (purple trace, Figure 2A), while only a ~0.5 kcal/mol difference was noted for *me*-FETE (orange trace, Figure 2A). The strong *syn* coplanar preference with the ester proximal to the furan, mirrors the *me*-FEFE derivative. In contrast, the ester group proximal to the thiophene ring in *me*-FETE leads only to a small energetic difference between the *syn* and *anti* coplanar forms, which may be due to attractive chalcogen-chalcogen interactions between the carbonyl oxygen and sulfur atom of the thiophene ring lowering the energy of the *anti* conformation.[16] Altogether, the computed torsional potentials suggest that conjugated macrocycles should be possible upon buildup into longer oligomers,

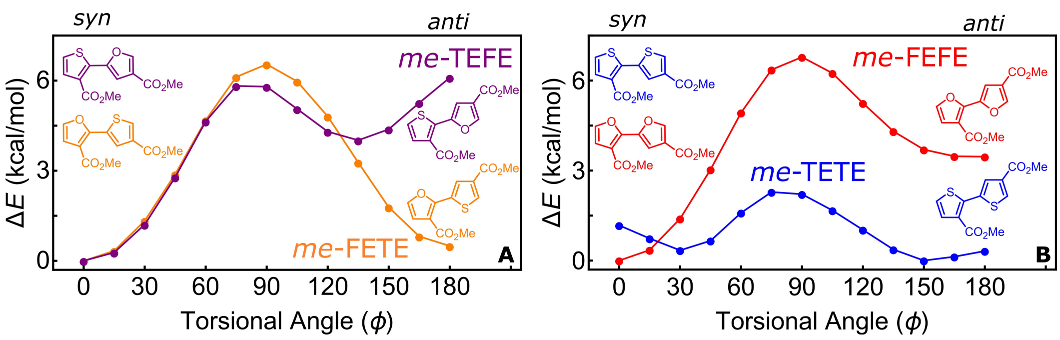

Figure 2. Torsional potential energy scans calculated at the B3LYP-D3(BJ)/6-31G(d,p) level for the hetero and homo dimers (**A** and **B**, respectively) of methyl furan 3-carboxylate and methyl thiophene 3-carboxylate.

though the weaker *syn* preference for one of the isomers is likely to impact the yield of the C4TE4FE macrocycle.

Monomer synthesis and macrocyclization

As shown in Scheme 1, two different ester-functionalized thiophene-furan dimers were synthesized to explore macrocyclization, mirroring the computed dimers but with hexyl ester side groups to ensure good solubility upon oligomerization. Suzuki–Miyaura coupling was first used to form the α-linked thiophene-furan dimers as shown in Scheme 1 with the commercially available [1,3-bis (2,6-diisopropylphenyl)imidazol-2-ylidene] (3-chloropyridyl)palladium (II) dichloride catalyst (PEPPSI-IPr).

A directed metalation with 2,2,6,6-tetramethylpiperidinylmagnesium chloride lithium chloride complex solution (TMPMgCl·LiCl) followed by electrophilic quenching with carbon tetrabromide (CBr_4) resulted in bromination proximal to the ester group, with TEFE–Br obtained in 58% yield and FETE–Br obtained in 85% yield. Installation of the pinacol boronic ester at the sterically accessible 5′-position was accomplished by an iridium-catalyzed borylation,[17] with Bpin–TEFE–Br obtained in 74% yield and Bpin–FETE–Br obtained in 64% yield. The two synthesized monomers, Bpin–TEFE–Br and Bpin–FETE–Br, were combined with three different commercially available catalysts: $Pd(PPh_3)_4$, Pd–G3–SPhos[18] and $Ni(COD)_2/PCy_3$ (Table 1, Entries 1–6). All reactions were carried out with 10 mol% catalyst and 2 equivalents of $K_3PO_4 \cdot H_2O$ in THF/water at 50 °C. The Bpin–FETE–Br monomer afforded higher yields in all instances as compared to Bpin–TEFE–Br (Table 1).

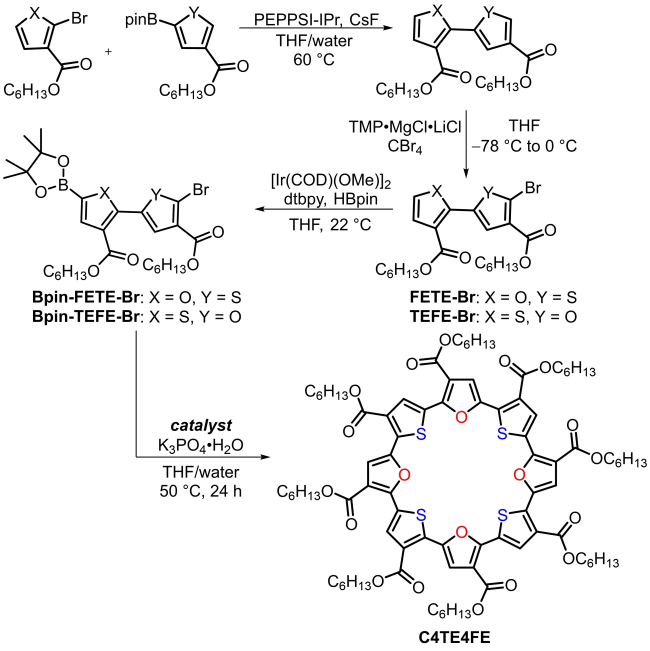

Bpin-FETE-Br: X = O, Y = S
Bpin-TEFE-Br: X = S, Y = O

FETE-Br: X = O, Y = S
TEFE-Br: X = S, Y = O

C4TE4FE

Scheme 1. Monomer synthesis and macrocyclization reaction.

Table 1. Catalyst choice for macrocyclization.[a]

Entry	Monomer	Catalyst (mol%)	Yield of C4TE4FE [%]
1	Bpin-TEFE-Br	$Pd(PPh_3)_4$ (10)	0
2	Bpin-TEFE-Br	Pd–G3–SPhos (10)	5
3	Bpin-TEFE-Br	$Ni(COD)_2$ (10), PCy_3 (20)	4
4	Bpin-FETE-Br	Pd–G3–SPhos (10)	9
5	Bpin-FETE-Br	$Pd(PPh_3)_4$ (10)	11
6	Bpin-FETE-Br	$Ni(COD)_2$ (10), PCy_3 (20)	11

[a] Typical reaction conditions: 0.35 mmol of monomer, 0.035 mmol of catalyst, 0.70 mmol of $K_3PO_4 \cdot H_2O$, 11.7 mL of THF:water (30:1), 50 °C, 24 h.

It is interesting to note that with Bpin-FETE–Br, each coupling event results in the formation of the strongly preferred *syn* conformer according to the computed torsional scans, which may be related to the higher yield with this monomer. For Bpin–TEFE–Br, yields ranged from 0–5% with the three catalyst systems, while with Bpin–FETE–Br, yields ranged from 9–11%. Though the yields are low to modest, the cyclization can be accomplished from the dimer and does not require laborious preparation via iterative coupling reactions.

Characterization

The formation of C4TE4FE was confirmed by MALDI-TOF mass spectrometry and NMR spectroscopy (Figures 3A and 3B). Observed isotope signals matched well with the predicted pattern as shown in Figure 3A. The powder X-ray scattering pattern, absorption spectrum, and cyclic voltammogram (CV) for C4TEFE are shown in Figure 3C–3E, along with the experimental data for the previously synthesized C6FE[6d] for reference. Two aromatic resonances are observed in the ^1H NMR spectrum of C4TE4FE, as expected for the equivalent thiophene and furan rings (8.72 and 7.89 ppm, H_A and H_B in Figure 3B). The diagnostic methylene protons of the hexyl ester side chains appear as a pair of overlapping triplets at 4.30 and 4.28 ppm ($^3J_{HH}=6.7$ and 7.0 Hz, H_C and H_D, Figure 3B). The ^{13}C NMR spectrum of C4TE4FE shown in the Supporting Information offered further confirmation of the macrocycle assignment with 22 total signals for the cyclic oligomer (8 aromatic, 12 aliphatic, and 2 carbonyl). A moderate ring strain energy was noted for *me*-C4TE4FE (12.5 kcal/mol), which was computed using a hyperhomodesmotic[19] reaction equation at the B3LYP-D3(BJ)/6-31G(d,p) IEFPCM(CH_2Cl_2) level (Figure S25).

C4TE4FE crystallized as both long thin needles and small plates from a liquid/liquid diffusion experiment where the macrocycle was dissolved in dichloromethane and layered with ethanol. Unfortunately, full structure determination using single crystal x-ray diffraction was not possible which may be due to the hexyl ester side chains. This is consistent with our previous work on C6FE where single crystal structure determination was not possible.[6d] Preliminary x-ray characterization was obtained by analysis of the crystalline solid using powder X-ray diffraction (Figure 3C) and it was compared to the all-furan derivative.

In both cases, a low q peak was observed at ~0.3 Å^{-1}, which corresponds to the distance (~21 Å) between macrocycles (governed primarily by the side chains). Bragg features in the

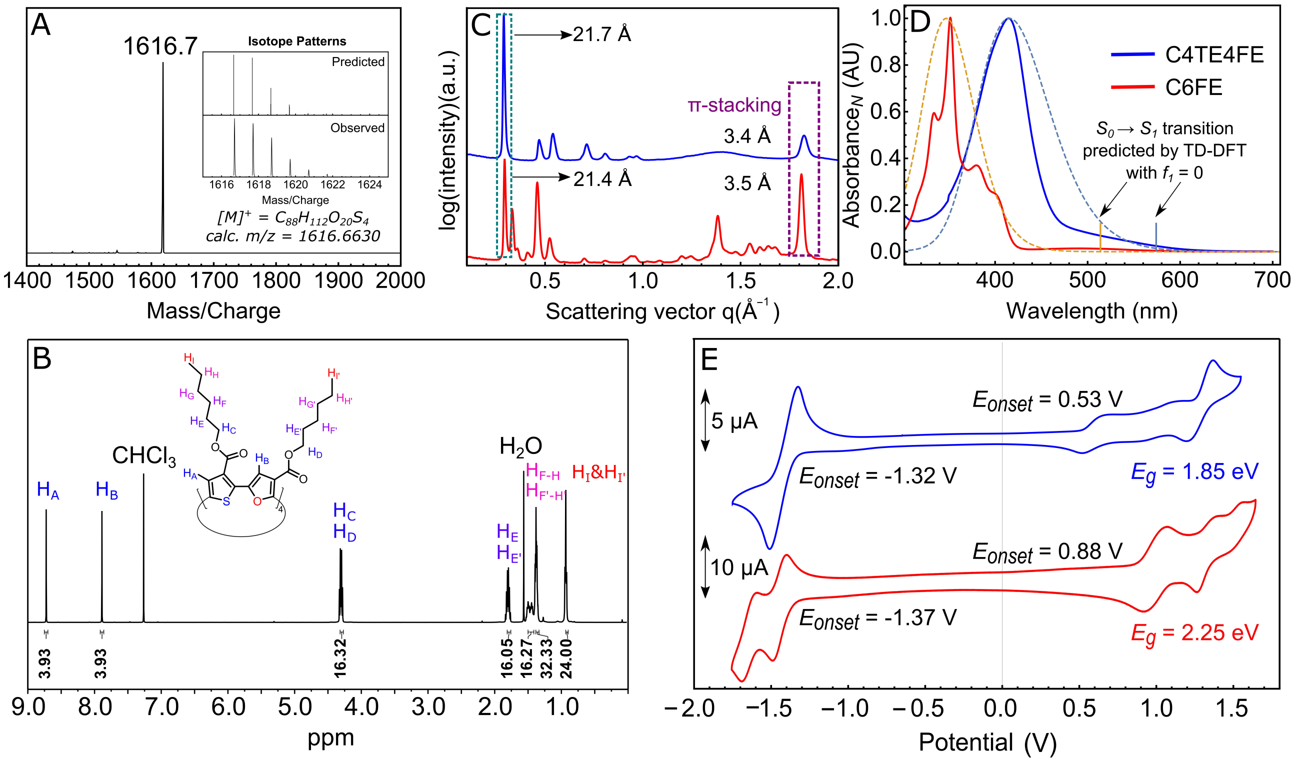

Figure 3. A) MALDI-TOF mass spectrum of C4TE4FE. B) ^{1}H NMR spectrum (500 MHz) of C4TE4FE collected at 25 °C in $CDCl_3$. C) Powder X-ray diffraction patterns for C4TE4FE (top, blue trace) and C6FE (bottom, red trace). D) Normalized UV-Vis absorption spectra of C4TE4FE (blue trace) and C6FE (red trace) collected in $CHCl_3$ and predicted by TD-DFT for *me*-C6FE and *me*-C4TE4FE (dashed lines, CAM-B3LYP/6-31G(d,p) IEFPCM(CH_2Cl_2)) E) Cyclic voltammograms of C4TE4FE (blue trace) and C6FE (red trace) in degassed CH_2Cl_2 (0.63 mg/mL) using NBu_4PF_6 as the supporting electrolyte (0.01 M for C4TE4FE and 0.07 M for C6FE), with a scan rate of 100 mV/s. The voltammogram was referenced using Fc/Fc$^+$ as an internal standard (0.46 V vs SCE).[21] Determination of the electrochemical band gap of C4TE4FE from the onsets of oxidation and reduction at +0.53 and −1.32 V respectively, yields a value of $E_g = 1.85$ eV.

mid q range (~1.4 Å^{-1}) can also be attributed to side chain packing. The sharp Bragg peaks in the mid q range for C6FE are indicative of more long-range order in this derivative, which is not surprising given the high degree of symmetry for this oligomer. Finally, intense π-stacking reflections were noted for both macrocycles with π-stacking distances of 3.4 Å and 3.5 Å for C4TE4FE and C6FE, respectively. Altogether, the powder patterns confirm that these materials are crystalline.

The UV-vis spectrum of C4TE4FE was assigned with the aid of time-dependent density functional theory (TD-DFT) calculations on *me*-C4TE4FE (dotted trace shown in Figure 3D). The HOMO–LUMO transition is predicted to have zero oscillator strength ($f_1 = 0$) and is shown as a vertical line in Figure 3D. The $S_0 \rightarrow S_2$ transition for C4TE4FE appears at 415 nm ($\varepsilon = 1.1 \times 10^5$ cm^{-1} M^{-1}). This value is in between the λ_{max} values for C8T and C10T at 396 and 424 nm, respectively.[12,20] It is also similar to the related cyclo[4]bifuran diimide which is comprised of 8 furan rings, with a $\lambda_{max} = 401$ nm.[6b] The symmetry forbidden $S_0 \rightarrow S_1$ transition for C4TE4FE appears at ~530 nm, near to the predicted transition at 574 nm. The low intensity for the symmetry forbidden $S_0 \rightarrow S_1$ is similar to observations for C8T and C10T. [12,20] The λ_{max} for C4TE4FE is red shifted by 60 nm when compared to C6FE, which is not surprising given the larger size of the macrocycle.

Cyclic voltammetry studies of C4TE4FE measured in CH_2Cl_2 versus the saturated calomel reference electrode (SCE) with NBu_4PF_6 as the supporting electrolyte revealed three quasi reversible oxidations at $E_{pa} = 0.67$ V, 1.14 and 1.37 V, respectively (blue trace in Figure 3E). The first oxidation potential sits nearly halfway between the reported oxidation potentials for cyclo[n]furans[6b] ($E_{pa} > 1.0$ V) and cyclo[n]thiophenes ($E_{pa} > 0.5$–0.6 V), demonstrating that the electronic structure of macrocycles can be tuned by altering the monomer composition. A single reduction potential was noted for C4TE4FE ($E_{pc} = -1.51$ V), while two reversible reductions were noted for C6FE ($E_{pc} = -1.49$ V and −1.70 V). Repeated scans suggested good redox stability for the alternating macrocycle, as the voltammogram was nearly identical with each repeated run.

The reduction noted for C4TE4FE is more cathodic than the related cyclo[4]bifurandiimide[6b] and cyclo[8]pyrrole[4b,c] (respectively −1.04 V and −0.08 V vs SCE). The cyclo[8]pyrrole is reported to have four 1e$^-$ oxidations and a 2e$^-$ reduction. C4TE4FE has a similar CV profile to cyclo[8]pyrrole with much larger current passed for reduction as compared to oxidation. It should also be noted that CVs for C4TE4FE were collected with low concentrations of supporting electrolyte (0.01 M), since higher concentrations led to a decrease in intensity for both oxidation and reduction peaks. We hypothesize that the C4TE4FE aggregates more strongly with increasing concentrations of NBu_4PF_6 in CH_2Cl_2, as the color of the solution darkens with increasing amounts of electrolyte.

To better understand the redox properties of C4TE4FE and C6FE, optimizations and frequency calculations for consecutive redox states were carried out at the B3LYP-D3(BJ)/6-31G(d,p) and ωB97xD/6-31G(d,p) levels using a continuum solvation model (IEFPCM) with CH_2Cl_2 as the solvent (Figure 4). Two functionals were used here as B3LYP has been noted to overestimate conjugation.[22] The energies relative to the neutral form are shown in the top of Figure 4. The ionization potentials (IP) and electron affinities (EA) for first and second redox steps were then computed by taking differences between consecutive steps as shown in the bottom of Figure 4. For the doubly oxidized/reduced states of both macrocycles, we considered singlet and triplet spin multiplicities as C10T has been reported to be a triplet upon double oxidation.[12]

The difference between the first oxidation (IP_1) and first reduction (EA_1) serves as an estimate of the computed bandgap and can be compared with the experimental data from cyclic voltammetry. As shown in Figure 4, the difference between the first ionization and reduction potential computed at the B3LYP-D3(BJ)/6-31G(d,p) IEFPCM(CH_2Cl_2) level was in excellent agreement with the electrochemical gap from cyclic voltammetry for both macrocycles (2.1 eV for *me*-C6FE and 1.8 eV for *me*-C4TE4FE).

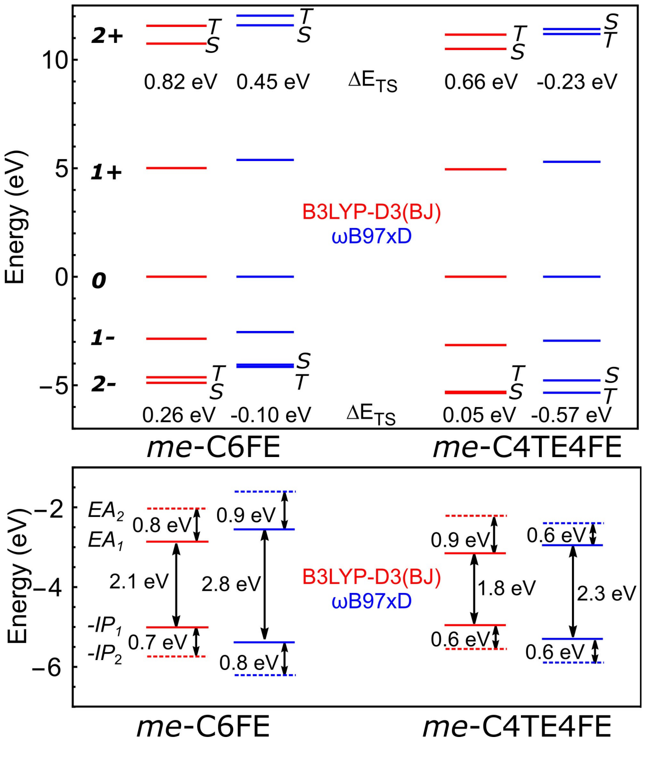

Figure 4. Total energies and frequency calculations were used to obtain Gibbs free energies (ΔG_f) for each computed structure. Top – Comparison of ΔG_f for computed redox states relative to the neutral macrocycle using either B3LYP-D3(BJ)/6-31G(d,p) or ωB97xD/6-31G(d,p) levels of theory with a continuum solvation model (IEFPCM) in CH_2Cl_2. The computed differences between the singlet and triplet multiplicities for the 2+ and 2− redox states are annotated on the plots ($\Delta E_{TS} = E_T - E_S$). Bottom – The computed differences correspond to each individual redox step where $IP_1 = \Delta G_f(0) - \Delta G_f(+1)$ and $EA_1 = \Delta G_f(-1) - \Delta G_f(0)$).

The gaps computed using the ωB97xD functional were roughly 0.5–0.7 eV higher than the experimentally determined values. Both levels of theory predict 0.6–0.9 eV differences between the first and second IPs and EAs which is larger than what is observed experimentally (Figure 3E).

The spin multiplicity after double oxidation of the macrocycle connects to a long-standing question in linear conjugated chains regarding the extent to which double oxidation results in two singly-charged polarons (triplet state) versus one doubly-charged bipolaron (singlet state).[23] As shown in Figure 4, the singlet state (denoted with *S*) or bipolaron is favored for both *me*-C6FE and *me*-C4TE4FE using the B3LYP-D3(BJ) functional. We then examined using computation how bipolaron formation impacts bonds lengths in cyclo[4]thiophene[4]furan (C4T4F) and the linear thiophene-furan octamer analog (L4T4F). Bond length alternation plots for $C4T4F^{2+}$ and $L4T4F^{2+}$ are shown in Figure 5. A repeating pattern is noted for the macrocycle, with the bond lengths for each thiophene and furan ring being the same, and the interring bonds being nearly equal around the cycle. This is very different from the linear analog, where the bond lengths of the individual heterocycles change from the center of the linear chain to the ends, suggesting charges are partially localized at the center for the linear derivative but delocalized in the cyclic variant.

Aromaticity

To examine aspects of aromaticity with *me*-$C6FE^{2+}$ and *me*-$C4TE4FE^{2+}$, DFT results were used to compute two aromaticity descriptors: the Nucleus Independent Chemical Shift (NICS)[24] and the Electron Localization Function (ELF).[25] The analysis of the isosurfaces of the ELF was carried out similarly to our previous work[6d] (Figures S29–30). Briefly, $ELF(r) = (1 + (D(r))/D_0(r)^2)^{-1}$ where $D(r)$ and $D_0(r)$ are determined from the total electron density and correspond, to the kinetic energy density due to Pauli repulsion and the Thomas-Fermi kinetic energy density. The Multiwfn wavefunction analysis package was used

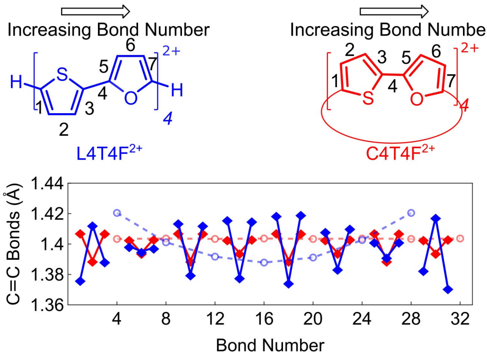

Figure 5. Bond alternation pathway calculated at the B3LYP-D3(BJ)/6-31G(d,p) level for a linear (in blue) and cyclic (in red) alternating thiophene-furan octamer. The open circles correspond to the interring bonds in each case.

to visualize π electron delocalization,[26] and calculations were carried out on combined electron densities from π-orbitals. The isosurface value which results in bifurcation of these orbitals around the cycle serves as an indicator of aromaticity, with the interring bond being key to delocalization between rings. An ELF_π value of 1 indicates perfect delocalization, and an $ELF_\pi = 0.7$ is normally considered a threshold for aromaticity.[25]

For *me*-C6FE and *me*-C4TE4FE, the ELF_π values for the interring bond in the neutral state are indicative of limited delocalization between heterocycles (0.51 and 0.54, respectively), consistent with the picture of a more local aromaticity for the heterocycles in the macrocycle. For both *me*-C6FE^{2+} and *me*-C4TE4FE^{2+}, ELF_π values greater than 0.7 were computed for the interring bond. This is consistent with more global aromatic character for the dications in each case.

For the NICS aromaticity criterion, negative values within the ring correspond to diatropic ring current (aromatic) and positive values correspond to paratropic ring current (antiaromaticity). Here, the zz components of NICS were computed at 1 Å above the plane of the macrocycle and values are reported in ppm and shown in Figure 6 ($NICS(1)_{zz}$). In this analysis, the individual furan rings for *me*-C6FE are aromatic ($NICS(1)_{zz} = -9.7$) while the center of the macrocycle itself is antiaromatic ($NICS(1)_{zz} = 17.1$). The NICS value for the individual furan rings in the macrocycle are lower than the value for methyl furan-3-carboxylate ($NICS(1)_{zz} = -24.1$, Figure S27). Upon double oxidation, an $NICS(1)_{zz} = -40.0$ is noted for each furan ring while the $NICS(1)_{zz}$ at the center of the macrocycle was −27.9, suggesting the cycle is globally aromatic (Figure 6). Similar effects were noted in the alternating *me*-C4TE4FE macrocycle, though some distinctions arise. First, the positive $NICS(1)_{zz}$ value (11.7) for the center of the alternating cycle is smaller than the calculated value for *me*-C6FE. In addition, the individual $NICS(1)_{zz}$ values for the furan and thiophene rings (−2.9 and −8.5, respectively) in the alternating cycle are smaller than the value computed for the furans in *me*-C6FE. The negative NICS value for the center of the *me*-C4TE4FE^{2+} suggests it is globally aromatic as denoted by the heat map plots in Figure 6 ($NICS(1)_{zz} = -32.1$). The darker blue for C4TE4FE does denote higher ring current for the larger ring, though caution must be used when comparing across these two systems given their different size.

We then examined whether chemical oxidation of C6FE and C4TE4FE would result in the predicted singlet dication. Both C6FE and C4TE4FE were treated with a slight excess of $SbCl_5$ in CD_2Cl_2 at room temperature in a glovebox (4 equiv.). In the case of C6FE, the reaction mixture became bright green while for C4TE4FE, the mixture became bright purple. Analysis of the reaction mixtures using ^1H NMR spectroscopy revealed remarkable downfield shifts for all protons in each case (Figure 6). Collection of the NMR spectra was an immediate indicator that triplet diradicals were unlikely, as it would be expected that linewidths would be broadened beyond detection in that case. It should be noted that some broadening was observed in the ^1H NMR spectrum of C6FE^{2+} which we suspect is due to incomplete double oxidation. Gidron and coworkers have noted with cyclo[4]furandiimide that reduction of the carbonyl groups enables facile chemical oxidation,[27] and a similar approach where the ester groups of C6FE are reduced may be needed here given the oxidation potentials of this system ($E_{pa} > 1.0$ V vs SCE). The lower oxidation potential of C4TE4FE is clearly a benefit in this case to achieve double oxidation.

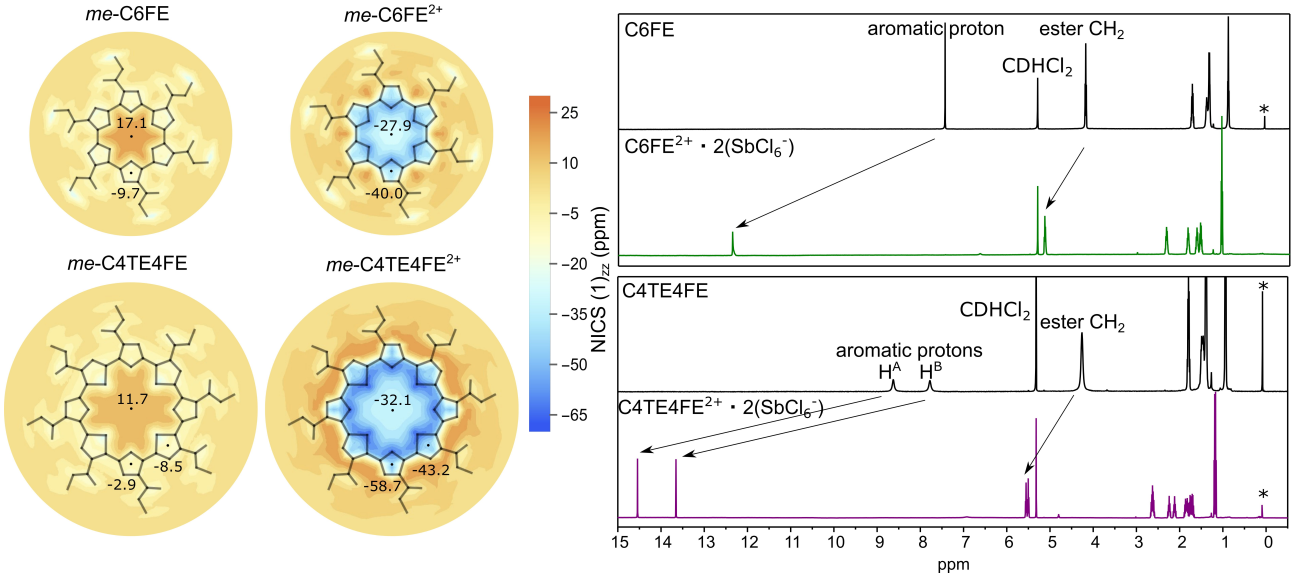

Figure 6. Left – $NICS(1)_{zz}$ plots for *me*-C6FE (top) and *me*-C4TE4FE (bottom) in their neutral and dication state. The color scale bar is shown where a more negative value corresponds to a higher degree of aromaticity in the encompassing ring, while a positive number corresponds to a higher degree of antiaromatic character. Macrocycles are annotated with NICS values at the center of the cycle and the heterocycles. The NMR-GIAO method was used with B3LYP-D3(BJ) functional and 6-31G(d,p) basis set on a polar grid placed 1 angstrom above the macrocycle plane to perform NICS calculations. Right – ^1H NMR spectra of neutral C6FE (top, black trace), $[C6FE]^{2+} \cdot 2(SbCl_6^-)$ (top, green trace), C4TE4FE (bottom, black trace), and $[C4TE4FE]^{2+} \cdot 2(SbCl_6^-)$ (bottom, purple trace) generated in situ in CD_2Cl_2 (an asterisk designates $SiMe_4$).

For C4TE4FE^{2+}, the two aromatic signals of the thiophene and furan rings had shifted downfield ~5.9 ppm, from 8.62 and 7.78 ppm to 14.55 and 13.66 ppm, respectively (Figure 6). The six signals in the aliphatic regions corresponding to the sidechain also shifted downfield, but by a much smaller amount than in the case of the aromatic protons. Computed NMR shielding tensors using the Gauge-Independent Atomic Orbital (GIAO) method for *me*-C4TE4FE suggest a downfield shift of more than 5 ppm for the aromatic protons upon double oxidation using B3LYP-D3(BJ)/6-31G(d,p) (Table S1). The change in ring current for the dication results in a large downfield shift for the aromatic protons of the thiophene and furan, providing strong evidence for global aromaticity. EPR studies of this reaction mixture also indicate minimal radical concentration for the doubly oxidized species, offering further confirmation that $[C4TE4FE]^{2+}\cdot 2(SbCl_6^-)$ exists in the singlet state (Figure S21).

Two sharp bands were observed in the UV-vis spectrum for $[C4TE4FE]^{2+}\cdot 2(SbCl_6^-)$ at $\lambda_{max} = 560$ and 1026 nm as shown in Figure 7 (predicted bands from TD-DFT shown as dotted line). Both the ^{1}H NMR and UV-vis spectra point to the dication as a singlet, and the spectrum closely resembles the previously reported [8]cyclo*para*phenylene dication[28] ([8]CPP^{2+}) with λ_{max} values of 528 nm and 1102 nm. Interestingly, it also matches closely with the reported spectrum for the C10T^{2+} with two bands at 683 nm and 1334 nm.[12]

After confirming that oxidation with $SbCl_5$ could take place, isolation of the dication was attempted. C4TE4FE was treated with 4 equivs. of $SbCl_5$ in degassed CH_2Cl_2 at room temperature in the glovebox and stirred for 5 min. The solvent was removed, and the resulting solid was washed with degassed hexanes. $[C4TE4FE]^{2+}\cdot 2(SbCl_6^-)$ was obtained as a dark purple solid in high yield. The ^{1}H NMR spectrum for the isolated $[C4TE4FE]^{2+}\cdot 2(SbCl_6^-)$ dication was nearly identical to that of the crude reaction mixture, suggesting complete oxidation. The purple solid was clearly air and moisture sensitive, but relatively stable as a solid under a N_2 atmosphere even after 1 month at −40 °C with no loss in color. We did note some minor radical contamination by EPR spectroscopy after dissolution of the dication in different solvents, suggesting higher sensitivity in solution.

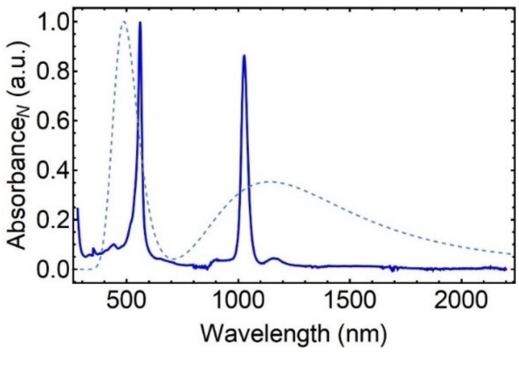

Figure 7. Normalized UV-vis-NIR absorption spectra of $[C4TE4FE]^{2+}\cdot 2(SbCl_6^-)$ in CH_2Cl_2 at 22 °C (Blue solid line) and predicted by TD-DFT for *me*-C4TE4FE^{2+} (dashed lines, CAM-B3LYP/6-31G(d,p) IEFPCM(CH_2Cl_2)).

Conclusion

In summary, a new class of heteroaromatic macrocycle, the cyclo[4]thiophene[4]furan was synthesized using Suzuki–Miyaura cross-coupling. This 8-membered macrocycle adds to the family of isolable cyclo[n]thiophenes and cyclo[n]furans whilst also expanding on the potential to make alternating sequences in conjugated cyclic molecules. A relatively small electrochemical bandgap of 1.85 eV was noted for cyclo[4]-thiophene[4]furan and chemical oxidation with $SbCl_5$ afforded an isolable dication. The aromaticity of the dication was probed using ^{1}H NMR and absorption spectroscopy, along with computation. The significant downfield shift for the aromatic protons of cyclo[4]thiophene[4]furan upon double oxidation was a clear indicator of a ring current change, and future work with these macrocycles will focus on obtaining a better understanding of the accessible redox states.

Altogether, we have demonstrated that our macrocyclization strategy using ester side chains as templating groups can be expanded to include other heterocycles in tandem with furan. Computational data was instrumental in detailed analysis of the redox chemistry of the cycle, while also pointing to aromaticity as a factor in stability of the singlet state over the triplet state upon double oxidation. This is a key consideration in the design of organic materials, as cyclic systems could lead to charge carriers with enhanced environmental stability. In the future, we anticipate exploring how other sequences may influence electronic properties of these flat conjugated macrocycles, as well as how they influence aggregation and organization in the solution and in the solid.

Acknowledgements

KJTN and TK are grateful to the NSF for support of this work (CHE-2109065). KJTN is also grateful to the ARO under which some initial results were obtained (W911NF-16-1-0053). The authors are also grateful to Yisong Guo and Mike Hendrich (Carnegie Mellon) for help with EPR measurements.

Conflict of Interests

The authors declare no conflict of interest.

Data Availability Statement

The data that support the findings of this study are available in the supplementary material of this article.

Keywords: conjugated macrocycles · cyclo[n]furans · cyclo[n]thiophenes · global aromaticity · homogeneous catalysis

[1] a) M. Iyoda, J. Yamakawa, M. J. Rahman, *Angew. Chem. Int. Ed.* **2011**, *50*, 10522–10553; b) M. Iyoda, H. Shimizu, *Chem. Soc. Rev.* **2015**, *44*, 6411–

6424; c) M. Ball, B. Zhang, Y. Zhong, B. Fowler, S. Xiao, F. Ng, M. Steigerwald, C. Nuckolls, *Acc. Chem. Res.* **2019**, *52*, 1068–1078; d) E. J. Leonhardt, R. Jasti, *Nat. Rev. Chem.* **2019**, *3*, 672–686.

[2] a) A. Muñoz-Castro, *Phys. Chem. Chem. Phys.* **2018**, *20*, 3433–3437; b) M. D. Peeks, M. Jirasek, T. D. W. Claridge, H. L. Anderson, *Angew. Chem. Int. Ed.* **2019**, *58*, 15717–15720; c) S. Eder, D.-J. Yoo, W. Nogala, M. Pletzer, A. S. Bonilla, A. J. P. White, K. E. Jelfs, M. Heeney, J. W. Choi, F. Glöcklhofer, *Angew. Chem. Int. Ed.* **2020**, *59*, 12958–12964; d) M. Rickhaus, M. Jirasek, L. Tejerina, H. Gotfredsen, M. D. Peeks, R. Haver, H.-W. Jiang, T. D. W. Claridge, H. L. Anderson, *Nat. Chem.* **2020**, *12*, 236–241; e) Z. Li, X. Hou, Y. Han, W. Fan, Y. Ni, Q. Zhou, J. Zhu, S. Wu, K.-W. Huang, J. Wu, *Angew. Chem. Int. Ed.* **2022**, *61*, e202210697.

[3] a) R. Jasti, J. Bhattacharjee, J. B. Neaton, C. R. Bertozzi, *J. Am. Chem. Soc.* **2008**, *130*, 17646–17647; b) H. Takaba, H. Omachi, Y. Yamamoto, J. Bouffard, K. Itami, *Angew. Chem. Int. Ed.* **2009**, *48*, 6112–6116; c) S. Yamago, Y. Watanabe, T. Iwamoto, *Angew. Chem. Int. Ed.* **2010**, *49*, 757–759; d) P. J. Evans, E. R. Darzi, R. Jasti, *Nat. Chem.* **2014**, *6*, 404–408; e) T. Kawanishi, K. Ishida, E. Kayahara, S. Yamago, *J. Org. Chem.* **2020**, *85*, 2082–2091.

[4] a) D. Seidel, V. Lynch, J. L. Sessler, *Angew. Chem. Int. Ed.* **2002**, *41*, 1422–1425; b) T. Köhler, D. Seidel, V. Lynch, F. O. Arp, Z. Ou, K. M. Kadish, J. L. Sessler, *J. Am. Chem. Soc.* **2003**, *125*, 6872–6873; c) M. Buda, A. Iordache, C. Bucher, J.-C. Moutet, G. Royal, E. Saint-Aman, J. L. Sessler, *Chem. Eur. J.* **2010**, *16*, 6810–6819.

[5] a) J. Krömer, I. Rios-Carreras, G. Fuhrmann, C. Musch, M. Wunderlin, T. Debaerdemaeker, E. Mena-Osteritz, P. Bäuerle, *Angew. Chem. Int. Ed.* **2000**, *39*, 3481–3486; b) G. Fuhrmann, T. Debaerdemaeker, P. Bäuerle, *Chem. Commun.* **2003**, 948–949; c) F. Zhang, G. Götz, H. D. F. Winkler, C. A. Schalley, P. Bäuerle, *Angew. Chem. Int. Ed.* **2009**, *48*, 6632–6635.

[6] a) O. Dishi, O. Gidron, *J. Org. Chem.* **2018**, *83*, 3119–3125; b) S. V. Mulay, O. Dishi, Y. Fang, M. R. Niazi, L. J. W. Shimon, D. F. Perepichka, O. Gidron, *Chem. Sci.* **2019**, *10*, 8527–8532; c) O. Dishi, P. Malakar, L. J. W. Shimon, S. Ruhman, O. Gidron, *Chem. Eur. J.* **2021**, *27*, 17794–17801; d) A. J. Varni, M. Kawakami, S. A. Tristram-Nagle, D. Yaron, T. Kowalewski, K. J. T. Noonan, *Org. Chem. Front.* **2021**, *8*, 1775–1782.

[7] a) O. Gidron, Y. Diskin-Posner, M. Bendikov, *J. Am. Chem. Soc.* **2010**, *132*, 2148–2150; b) O. Gidron, N. Varsano, L. J. W. Shimon, G. Leitus, M. Bendikov, *Chem. Commun.* **2013**, *49*, 6256–6258; c) S. Sharma, M. Bendikov, *Chem. Eur. J.* **2013**, *19*, 13127–13139; d) X.-H. Jin, D. Sheberla, L. J. W. Shimon, M. Bendikov, *J. Am. Chem. Soc.* **2014**, *136*, 2592–2601; e) S. Sharma, N. Zamoshchik, M. Bendikov, *Isr. J. Chem.* **2014**, *54*, 712–722; f) J. W. G. Bloom, S. E. Wheeler, *J. Chem. Theory Comput.* **2014**, *10*, 3647–3655.

[8] A. J. Varni, A. Fortney, M. A. Baker, J. C. Worch, Y. Qiu, D. Yaron, S. Bernhard, K. J. T. Noonan, T. Kowalewski, *J. Am. Chem. Soc.* **2019**, *141*, 8858–8867.

[9] a) T.-T. Bui, A. Iordache, Z. Chen, V. V. Roznyatovskiy, E. Saint-Aman, J. M. Lim, B. S. Lee, S. Ghosh, J.-C. Moutet, J. L. Sessler, D. Kim, C. Bucher, *Chem. Eur. J.* **2012**, *18*, 5853–5859; b) Z. Zhang, J. M. Lim, M. Ishida, V. V. Roznyatovskiy, V. M. Lynch, H.-Y. Gong, X. Yang, D. Kim, J. L. Sessler, *J. Am. Chem. Soc.* **2012**, *134*, 4076–4079; c) Z. Zhang, W.-Y. Cha, N. J. Williams, E. L. Rush, M. Ishida, V. M. Lynch, D. Kim, J. L. Sessler, *J. Am. Chem. Soc.* **2014**, *136*, 7591–7594; d) I.-T. Ho, Z. Zhang, M. Ishida, V. M. Lynch, W.-Y. Cha, Y. M. Sung, D. Kim, J. L. Sessler, *J. Am. Chem. Soc.* **2014**, *136*, 4281–4286; e) H. Ito, Y. Mitamura, Y. Segawa, K. Itami, *Angew. Chem. Int. Ed.* **2015**, *54*, 159–163; f) T. Iwanaga, Y. Yamada, T. Yamauchi, Y. Misaki, M. Inoue, H. Yamada, *Chem. Lett.* **2018**, *47*, 760–762; g) T. C. Lovell, C. E. Colwell, L. N. Zakharov, R. Jasti, *Chem. Sci.* **2019**, *10*, 3786–3790; h) C. Li, C. Wang, Y. Guo, Y. Jin, N. Yao, Y. Wu, F. Zhang, W. Li, *J. Mater. Chem. C* **2019**, *7*, 3802–3810; i) T. C. Lovell, Z. R. Garrison, R. Jasti, *Angew. Chem. Int. Ed.* **2020**, *59*, 14363–14367; j) M. Hermann, D. Wassy, B. Esser, *Angew. Chem. Int. Ed.* **2021**, *60*, 15743–15766.

[10] a) M. K. Cyrański, T. M. Krygowski, M. Wisiorowski, N. J. R. van Eikema Hommes, P. R. Schleyer, *Angew. Chem. Int. Ed.* **1998**, *37*, 177–180; b) N. Toriumi, A. Muranaka, E. Kayahara, S. Yamago, M. Uchiyama, *J. Am. Chem. Soc.* **2015**, *137*, 82–85; c) C. Liu, Y. Ni, X. Lu, G. Li, J. Wu, *Acc. Chem. Res.* **2019**, *52*, 2309–2321; d) S. M. Kopp, H. Gotfredsen, J.-R. Deng, T. D. W. Claridge, H. L. Anderson, *J. Am. Chem. Soc.* **2020**, *142*, 19393–19401; e) R. Ayub, O. El Bakouri, J. R. Smith, K. Jorner, H. Ottosson, *J. Phys. Chem. A* **2021**, *125*, 570–584; f) R. Lingas, N. D. Charistos, A. Muñoz-Castro, *ChemPhysChem* **2021**, *22*, 741–751; g) M. D. Ambhore, S. P. Panchal, A. Mondal, S. Konar, V. G. Anand, *Org. Biomol. Chem.* **2022**, *20*, 2818–2821.

[11] S. S. Zade, M. Bendikov, *J. Org. Chem.* **2006**, *71*, 2972–2981.

[12] F. Zhang, G. Götz, E. Mena-Osteritz, M. Weil, B. Sarkar, W. Kaim, P. Bäuerle, *Chem. Sci.* **2011**, *2*, 781–784.

[13] a) J. B. Lin, Y. Jin, S. A. Lopez, N. Druckerman, S. E. Wheeler, K. N. Houk, *J. Chem. Theory Comput.* **2017**, *13*, 5624–5638; b) V. Topolskaia, A. A. Pollit, S. Cheng, D. S. Seferos, *Chem. Eur. J.* **2021**, *27*, 9038–9043.

[14] S. Grimme, S. Ehrlich, L. Goerigk, *J. Comput. Chem.* **2011**, *32*, 1456–1465.

[15] S. S. Zade, M. Bendikov, *Chem. Eur. J.* **2007**, *13*, 3688–3700.

[16] H. Huang, L. Yang, A. Facchetti, T. J. Marks, *Chem. Rev.* **2017**, *117*, 10291–10318.

[17] G. A. Chotana, V. A. Kallepalli, R. E. Maleczka, M. R. Smith, *Tetrahedron* **2008**, *64*, 6103–6114.

[18] N. C. Bruno, M. T. Tudge, S. L. Buchwald, *Chem. Sci.* **2013**, *4*, 916–920.

[19] S. E. Wheeler, K. N. Houk, P. R. Schleyer, W. D. Allen, *J. Am. Chem. Soc.* **2009**, *131*, 2547–2560.

[20] E. Mena-Osteritz, F. Zhang, G. Götz, P. Reineker, P. Bäuerle, *Beilstein J. Nanotechnol.* **2011**, *2*, 720–726.

[21] N. G. Connelly, W. E. Geiger, *Chem. Rev.* **1996**, *96*, 877–910.

[22] T. Körzdörfer, J. L. Brédas, *Acc. Chem. Res.* **2014**, *47*, 3284–3291.

[23] a) M. G. Hill, K. R. Mann, L. L. Miller, J.-F. Penneau, *J. Am. Chem. Soc.* **1992**, *114*, 2728–2730; b) M. G. Hill, J.-F. Penneau, B. Zinger, K. R. Mann, L. L. Miller, *Chem. Mater.* **1992**, *4*, 1106–1113; c) Y. Furukawa, *Synth. Met.* **1995**, *69*, 629–632; d) A. J. W. Tol, *Synth. Met.* **1995**, *74*, 95–98; e) A. J. W. Tol, *Chem. Phys.* **1996**, *208*, 73–79; f) Y. Yu, E. Gunic, B. Zinger, L. L. Miller, *J. Am. Chem. Soc.* **1996**, *118*, 1013–1018; g) S. Irle, H. Lischka, *J. Chem. Phys.* **1997**, *107*, 3021–3031; h) D. D. Graf, R. G. Duan, J. P. Campbell, L. L. Miller, K. R. Mann, *J. Am. Chem. Soc.* **1997**, *119*, 5888–5899; i) J. A. E. H. van Haare, E. E. Havinga, J. L. J. van Dongen, R. A. J. Janssen, J. Cornil, J. L. Brédas, *Chem. Eur. J.* **1998**, *4*, 1509–1522; j) V. M. Geskin, J. L. Brédas, *ChemPhysChem* **2003**, *4*, 498–505; k) N. Zamoshchik, U. Salzner, M. Bendikov, *J. Phys. Chem. C* **2008**, *112*, 8408–8418; l) R. Shomura, K. Sugiyasu, T. Yasuda, A. Sato, M. Takeuchi, *Macromolecules* **2012**, *45*, 3759–3771.

[24] Z. Chen, C. S. Wannere, C. Corminboeuf, R. Puchta, P. R. Schleyer, *Chem. Rev.* **2005**, *105*, 3842–3888.

[25] a) J. Poater, M. Duran, M. Solà, B. Silvi, *Chem. Rev.* **2005**, *105*, 3911–3947; b) J. C. Santos, W. Tiznado, R. Contreras, P. Fuentealba, *J. Chem. Phys.* **2004**, *120*, 1670–1673.

[26] a) T. Lu, F.-W. Chen, *Acta Phys. -Chim. Sin.* **2011**, *27*, 2786–2792; b) T. Lu, F. Chen, *J. Comput. Chem.* **2012**, *33*, 580–592.

[27] O. Dishi, Y. Rahav, R. Carmieli, O. Gidron, *Chem. Eur. J.* **2022**, *28*, e202202082.

[28] E. Kayahara, T. Kouyama, T. Kato, H. Takaya, N. Yasuda, S. Yamago, *Angew. Chem. Int. Ed.* **2013**, *52*, 13722–13726.

Manuscript received: February 14, 2023
Accepted manuscript online: April 10, 2023
Version of record online: ■■, ■■

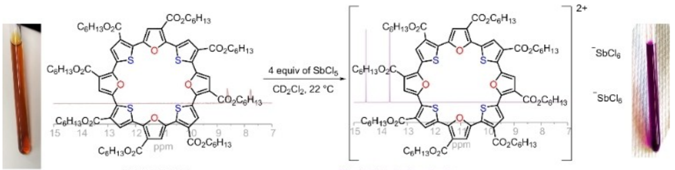

C4TE4FE

✓ Isolatable in the glovebox
✓ stable more than 30 days in the solid state under N_2

An alternating furan-thiophene macrocycle has been synthesized without the need for stepwise buildup of oligomers. The ring is weakly antiaromatic due to the 4n π electrons along the outer annulene pathway of carbon atoms. The macrocycle can be made globally aromatic through chemical oxidation with $SbCl_5$.

M. Kawakami, D. Sharma, Dr. A. J. Varni, Prof. S. Tristram-Nagle, Prof. D. Yaron, Prof. T. Kowalewski, Prof. K. J. T. Noonan**

1 – 9

Design, Synthesis and Aromaticity of an Alternating Cyclo[4]Thiophene[4]-Furan